



# Karbala International Journal of Modern Science

Manuscript 3391

## Computational Investigation of the Unveils NSD2 Inhibition Potential of Berberis vulgaris, Sambucus nigra, and Morus alba through Virtual Screening, Molecular Docking, MD Simulation, and DFT Analyses

Supriyo Saha

Vanshita Gupta

Ahad Hossain

Prinsa Prinsa

Jannatul Ferdous

See next page for additional authors

Follow this and additional works at: <https://kijoms.uokerbala.edu.iq/home>

 Part of the [Biology Commons](#), [Chemistry Commons](#), [Computer Sciences Commons](#), and the [Physics Commons](#)

---

# Computational Investigation of the Unveils NSD2 Inhibition Potential of *Berberis vulgaris*, *Sambucus nigra*, and *Morus alba* through Virtual Screening, Molecular Docking, MD Simulation, and DFT Analyses

## Abstract

Nuclear receptor binding set domain protein 2 (NSD2) plays a key role in chromatin regulation and is associated with different cancers and other developmental problems. Berries are rich in major secondary metabolites with anticancer properties. Here, we virtually screened 145 berry phytochemicals as putative NSD2 inhibitors via structure-based virtual screening, molecular docking, MD simulations, and DFT and ADMET analyses. Among them,  $\alpha$ -carotene had the maximum docking score of -9.9 kcal/mol, followed by sulfuretin and  $\beta$ -amyryn. MD simulation analysis revealed that the dynamic behavior of the ligand–NSD2 complexes was within the limit, indicating no significant changes in the structural integrity of the ligand upon interaction with the receptor. DFT studies have indicated that  $\alpha$ -carotene is the most stable and reactive molecule, followed by sulfuretin and  $\beta$ -amyryn. These molecules respect the minimum criteria of Lipinski's rule with acceptable ADMET profiles. These data suggest that these phytochemicals may play a role in the inhibition of the NSD2 protein and associated cancers. The selected phytochemicals  $\alpha$ -carotene, sulfuretin and  $\beta$ -amyryn are abundant in *Berberis vulgaris* (barberry), *Sambucus nigra* (elder berry), and *Morus alba* (white mulberry). *Berberis vulgaris*, *Sambucus nigra*, and *Morus alba* have shown efficient anticancer properties. Therefore, establishing these phytoconstituents via *in vitro* and *in vivo* experiments could be beneficial for humankind.

## Keywords

Berries metabolites; NSD2 inhibitors; Virtual screening; Molecular docking; MD simulation; DFT.

## Creative Commons License



This work is licensed under a [Creative Commons Attribution-Noncommercial-No Derivative Works 4.0 License](https://creativecommons.org/licenses/by-nc-nd/4.0/).

## Authors

Supriyo Saha, Vanshita Gupta, Ahad Hossain, Prinsa Prinsa, Jannatul Ferdous, Kiran Bharat Lokhande, Vikash Jakhmola, and Sarkar M. A. Kawsar

## RESEARCH PAPER

# Computational Investigation of the Unveils NSD2 Inhibition Potential of *Berberis vulgaris*, *Sambucus nigra*, and *Morus alba* Through Virtual Screening, Molecular Docking, MD Simulation, and DFT Analyses

Supriyo Saha <sup>a</sup>, Vanshita Gupta <sup>a</sup>, Ahad Hossain <sup>b</sup>, Prinsa <sup>c</sup>, Jannatul Ferdous <sup>b</sup>, Kiran B. Lokhande <sup>d</sup>, Vikash Jakhmola <sup>a</sup>, Sarkar M.A. Kawsar <sup>b,\*</sup>

<sup>a</sup> Department of Pharmaceutical Chemistry, Uttaranchal Institute of Pharmaceutical Sciences, Uttaranchal University, Dehradun, 248001, Uttarakhand, India

<sup>b</sup> Laboratory of Carbohydrate and Nucleoside Chemistry (LCNC), Department of Chemistry, Faculty of Science, University of Chittagong, Chittagong, 4331, Bangladesh

<sup>c</sup> Department of Pharmaceutical Chemistry, Siddhartha Institute of Pharmacy, Near IT-Park, Sahastradhara Road, Dehradun, 248001, Uttarakhand, India

<sup>d</sup> BRIC-Translational Health Science and Technology Institute (THSTI), Faridabad, Haryana, India

## Abstract

Nuclear receptor binding set domain protein 2 (NSD2) plays a key role in chromatin regulation and is associated with different cancers and other developmental problems. Berries are rich in major secondary metabolites with anticancer properties. Here, we virtually screened 145 berry phytochemicals as putative NSD2 inhibitors via structure-based virtual screening, molecular docking, MD simulations, and DFT and ADMET analyses. Among them,  $\alpha$ -carotene had the maximum docking score of  $-9.9$  kcal/mol, followed by sulfuretin and  $\beta$ -amyrin. MD simulation analysis revealed that the dynamic behavior of the ligand–NSD2 complexes was within the limit, indicating no significant changes in the structural integrity of the ligand upon interaction with the receptor. DFT studies have indicated that  $\alpha$ -carotene is the most stable and reactive molecule, followed by sulfuretin and  $\beta$ -amyrin. These molecules respect the minimum criterion of Lipinski's rule with acceptable ADMET profiles. These data suggest that these phytochemicals may play a role in the inhibition of the NSD2 protein and associated cancers. The selected phytochemicals  $\alpha$ -carotene, sulfuretin and  $\beta$ -amyrin are abundant in *Berberis vulgaris* (barberry), *Sambucus nigra* (elder berry), and *Morus alba* (white mulberry). *Berberis vulgaris*, *Sambucus nigra*, and *Morus alba* have shown efficient anticancer properties. Therefore, establishing these phytoconstituents via *in vitro* and *in vivo* experiments could be beneficial for humankind.

**Keywords:** Berries metabolites, NSD2 inhibitors, Virtual screening, Molecular docking, MD simulation, DFT

## 1. Introduction

The incidence of multiple types of cancer is increasing rapidly, and resistance to therapies makes finding inhibitors challenging. Many receptors, such as KRAS [1] and NSD, are targeted for inhibitory activities. Nuclear receptor binding set

domain protein 2 (NSD2), also known as WHSC1/MMSET, is a gene belonging to the family of histone 3 lysine 36 (H3k36) methyltransferases [2]. The NSD family (NSD1, NSD2, and NSD3) plays an important role in chromatin regulation and has been implicated in developmental syndromes and numerous cancers [3]. NSD2 encodes a protein with several

Received 21 September 2024; revised 16 December 2024; accepted 19 December 2024.  
Available online 18 January 2025

\* Corresponding author.  
E-mail address: akawsarabe@yahoo.com (S.M.A. Kawsar).

<https://doi.org/10.33640/2405-609X.3391>

2405-609X/© 2025 University of Kerbala. This is an open access article under the CC-BY-NC-ND license (<http://creativecommons.org/licenses/by-nc-nd/4.0/>).

important domains, such as the proline-tryptophan-tryptophan-proline (PWWP), plant homeodomain (PHD), and methyltransferase domains [4]. PWWP1 and PWWP2 are two subtypes with the ability to bind both DNA and histones. The NSD2 protein is located on chromosome 4p16 and regulates chromatin through H3K36 and H4K20 methylation, which also promotes the metastatic behavior of prostate cancer [5]. Although the underlying regulatory mechanism is still unknown, its *in vitro* substrate specificity has been expanded to include H3K4, H3K9, H3K27, H3K36, H3K79, and H4K20. The overexpression of NSD2 causes cell division and changes how gene expression levels are regulated. Abnormal expression of NSD2 is associated with epithelial–mesenchymal transition, cancer cell metastasis and multiple myeloma due to recurrent (4; 14) chromosomal translocation. Studies have shown the direct connection of NSD2 with lung adenocarcinoma (LUAD) and blood cancer. An NSD2 variant [NSD2.pGlu1099Lys (p.E1099K) previously unknown] was identified in a non-translocated acute lymphoblastic leukemia (ALL) cell line that shares chromatin. NSD2 interacts with  $\beta$ -catenin, GTPase-activating protein 1 (IQGAP1), TIAM Rac1-linked GEF 1, and GTPase-activating protein 1 (TIAM1). IQGAP1 and TIAM1 are two functionally interacting proteins [6]. Misexpression of the variant induced a chromatin characteristic of NSD2 hyperactivation and promoted transformation. The overexpression of NSD2 is associated with 15 different cancer types [7]. The inhibition of NSD2 affects apoptosis and inhibits cell proliferation. Some natural sources have inhibited the effects of sinefungin on NSD2. Sinefungin is an adenosyl derivative of ornithine with antifungal and antimicrobial properties. This natural nucleoside is located in *Streptomyces* and is related to S-adenosylmethionine. Other NSD2 inhibitors include SCHEMBL22981317 (PubChem CID 156069450), and CHEMBL5186268 (PubChem CID 164517136) with IC<sub>50</sub> values of 0.0055  $\mu$ M, and 0.11  $\mu$ M, respectively. Another virtually screened NSD2 inhibitor 7-(5-methyl-3-(2-methyl-5-(piperidin-1-ylmethyl)phenyl)isoxazol-4-yl)-2H-benzo[b][1,4]oxazin-3(4H)-one has shown good potent activity [8,9]. The use of new NSD2 inhibitors from natural sources is highly promising. Many studies have reported the relationships between natural sources and health benefits. Virtual screening is the process of identifying suitable chemical structures from the mining of chemical libraries. 9-[2-(4-bromophenoxy)ethyl]-9H-purin-6-amine showed potent NSD2 inhibition. Berries from small shrubs and large trees contain several secondary metabolites that positively impact

human health. Berries contain flavonoids, terpenoids, phenol glycosides, vitamins, and antioxidants in all parts of the plant, whereas some contain these compounds only in particular parts, such as fruits, seeds, and leaves [10]. Bioactive compounds from berries are reported to have positive anti-inflammatory and antioxidant effects [11]. The primary components of the health benefits of these berries are thought to be flavonoids and phenolics, which are notable for their ability to prevent cardiovascular diseases, lower inflammation, enhance immune system performance, improve neurological function, and provide resistance against oxidative stress [12]. In this work, we computationally established the role of phytoconstituents of berries against NSD2 by computational methods such as molecular docking, MD simulation, DFT and ADMET analysis. The experimental framework of the current work is illustrated in Fig. S1 ([https://kijoms.uokerbala.edu.iq/cgi/editor.cgi?article=3391&window=additional\\_files&context=home](https://kijoms.uokerbala.edu.iq/cgi/editor.cgi?article=3391&window=additional_files&context=home)).

## 2. Materials and methods

### 2.1. Protein system preparation

The crystal structure of the histone-lysine N-methyltransferase PWWP1 domain of the NSD2 protein (PDB ID: 6UE6) in complex with MR837 was procured from the RCSB protein data bank ([www.rcsb.org](http://www.rcsb.org)). The resolution of the receptor was 2.40. A Ramachandran plot of the NSD2 protein confirmed that 113 amino acid residues (97.4%) and 03 amino acid residues (2.6%) are under the most favored and additional allowed regions, respectively [13,14]. The RMSD value of the C $\alpha$  of the NSD2 protein lies within 2. In the structure, 24.05% and 18% of the regions were helix and strand, respectively. There was no overlap between the helix and strands. Drug discovery Studio Visualizer was used to determine the key residues within the active sites. The latter results revealed that the reference co-crystallized molecules interact with ALA 54 by hydrogen bonding interactions; VAL 14, TYR 17, TRP 20, PHE 50, and ALA 58 *via* hydrophobic interactions; and PHE 51, GLY 52, ASP 53, PRO 55, GLU 56, LEU 102, and GLN 105 by van der Waals interactions (Fig S2). These residues were used to determine the grid-box dimensions for the molecular docking procedures.

### 2.2. Preparation of ligand molecules

An in-house chemical library of 145 key phytochemicals from berries was generated through

an extensive literature search. Then, Avogadro software (Table S1) ([https://kijoms.uokerbala.edu.iq/cgi/editor.cgi?article=3391&window=additional\\_files&context=home](https://kijoms.uokerbala.edu.iq/cgi/editor.cgi?article=3391&window=additional_files&context=home)) was used to develop all the phytochemicals, MR837, and the standard Lem-14 [15]. The MMFF94 force field and steepest descent techniques were used to optimize the molecules [16].

### 2.3. Molecular docking parameters of the molecules interacting with the receptors

The ligand and receptor molecules were subjected to Gasteiger charges and then saved in PDBQT format [17]. The Lamarckian genetic method was used to identify the best ligand binding site inside each protein [18]. BioVIA Discovery Studio Visualizer 4.5 was utilized to visually represent and examine the docking data. Center\_x = 36.697, center\_y = 66.518, and center\_z = 101.463 were the grid box dimensions for the NSD2 receptor, with exhaustiveness = 8.

### 2.4. Molecular dynamic (MD) simulations

The structural and dynamic changes in a ligand and protein complex can be efficiently determined via molecular dynamic simulation [19,20]. This work examined the thermodynamic properties of the ligand–receptor combination using Schrodinger's Desmond program (Schrodinger Release 2019-4: Desmond). In this process, missing loops and missing side chains are added to the protein–ligand complex, followed by the deletion of water molecules [21]. At pH 7.0, all the hydrogen bonds were assigned within the complex. The OPLS2005 force field was used for the energy minimization process [22]. The receptor–ligand complex was solvated in a cubic box with a buffer size of 10 Å and a periodic boundary condition to an infinite system via the explicit three-point (TIP3) water model. Table S2 ([https://kijoms.uokerbala.edu.iq/cgi/editor.cgi?article=3391&window=additional\\_files&context=home](https://kijoms.uokerbala.edu.iq/cgi/editor.cgi?article=3391&window=additional_files&context=home)) displays the total quantity of water molecules and counterions utilized in the neutralization of the drug–receptor complex. Using the OPLS-2005 force field, energy minimization of the complicated system was achieved by the steepest descent approach. All the molecular dynamics (MD) simulations were performed with Schrodinger's Desmond software, with the OPLS-2005 force field. All systems were minimized using the steepest descent algorithm and then subjected to a 10 ps NVT equilibration, a 100 ps NPT equilibration, and a 100 ns NPT production run. A leapfrog

integrator with a 2-fs time step was used throughout. Using the M-SHAKE technique, the bond lengths of every hydrogen atom were constrained. The RMSD and RMSF graphs were subsequently processed and the amino acid variations of the receptor following its interaction with the ligand molecules were computed. Contact calculations were also performed for protein–ligand interactions.

### 2.5. Frontier molecular orbital (FMO) analysis

The electronic characteristics of  $\alpha$ -carotene,  $\beta$ -amyryn, and sulfuretin were estimated using Beck's (B) three-parameter hybrid model and Lee, Yang, and Parr's (LYP) correlation functional with the B3LYP/6-31G (d,p) basis set [23]. A bonding orbital is denoted by the acronym HOMO, which represents the highest occupied molecular orbital. LUMO, on the other hand, stands for the lowest unoccupied molecular orbital, and it describes orbitals that are opposed to bonding [24,25]. The energies of all bonding orbitals are negative, and the energies of all antibonding orbitals are positive. This is due to the definition of zero energy as a nonbonded state, wherein antibonding orbitals have a greater energy than zero and bonding orbitals have a lower energy than zero. Most nonbonding orbitals have energies that are zero or very close to zero. An electron acceptor is the leading empty innermost orbital (LUMO) that is not occupied by electrons [26]. Here, we used GAMESS software to conduct an FMO analysis, and WxMacMolPlt (version 7.7.3) was used to show the results [27]. The global chemical reactivity was calculated via analysis of the molecular orbital characteristics using the following equations.

$$\text{Gap} (\Delta\varepsilon) = \varepsilon_{\text{LUMO}} - \varepsilon_{\text{HOMO}}; \eta = \frac{[\varepsilon_{\text{LUMO}} - \varepsilon_{\text{HOMO}}]}{2}; S = \frac{1}{\eta}; \mu = \frac{[\varepsilon_{\text{LUMO}} + \varepsilon_{\text{HOMO}}]}{2}; \chi = -\frac{[\varepsilon_{\text{LUMO}} + \varepsilon_{\text{HOMO}}]}{2}; \omega = \frac{\mu^2}{2\eta}$$

where, chemical potential ( $\mu$ ), electronegativity ( $\chi$ ) and electrophilicity ( $\omega$ ) are related to the HOMO and LUMO energies ( $\varepsilon$ ), hardness ( $\eta$ ), and softness ( $S$ ).

### 2.6. Molecular electrostatic potential (MEP) investigation

MEP map analysis is a potent technique for comprehending the electronic characteristics of molecules and forecasting their biological and chemical activities [28]. The various colors of the electrostatic potential represent various values. As the assault zone moves through the colors blue, green, yellow, orange, and red, its potentiality

diminishes [29]. The red zone denotes the largest negative region, where electrophiles can attack quickly, and the blue zone denotes the entire positive area, which is appropriate for nucleophilic attack. Additionally, the green hue indicates that there are no possible zones. The MEPs of  $\beta$ -amyirin, sulfuretin, and  $\alpha$ -carotene were calculated at the B3LYP/6-31G(d,p) level of theory using the GAMESS software (version R2 released on June 30, 2024).

### 2.7. Calculation of drug likelihood

ADMET data of the phytoconstituents were calculated using Swiss ADME ([www.swissadme.ch/index.php](http://www.swissadme.ch/index.php) accessed on 30 May 2024) and Osiris version 2.9.1, respectively [30,31].

## 3. Results and discussion

### 3.1. Molecular docking of phytoconstituents from berries with the NSD2 protein

A total of 145 phytoconstituents from different species of berries were screened for the NSD2 protein. Compared with the standard synthetic heterocyclic compounds Lem-14 (Dock score:  $-9.9$  kcal/mol),  $\alpha$ -carotene, sulfuretin and  $\beta$ -amyirin presented the highest docking scores of  $-9.9$  kcal/mol,  $-9.4$  kcal/mol, and  $-9.3$  kcal/mol, respectively, and achieved the top three ranks among all docked molecules (Table S3) ([https://kijoms.uokerbala.edu.iq/cgi/editor.cgi?article=3391&window=additional\\_files&context=home](https://kijoms.uokerbala.edu.iq/cgi/editor.cgi?article=3391&window=additional_files&context=home)) [32,33]. Our molecular docking focused on targeting the drug-compatible NSD2-PWWP1 domain [34].

The key residues lining the active site of the NSD2 protein include PHE51, GLY52, ASP53, LEU102, GLN105, ALA54, VAL14, TYR17, TRP20, PHE50, and ALA58. The latter is a known inhibitor of NSD2 with an  $IC_{50}$  of  $132 \mu\text{M}$  [35]. The molecular docking data for all the bioactive molecules are shown in Table S4 ([https://kijoms.uokerbala.edu.iq/cgi/editor.cgi?article=3391&window=additional\\_files&context=home](https://kijoms.uokerbala.edu.iq/cgi/editor.cgi?article=3391&window=additional_files&context=home)). Interaction analysis between these molecules and NSD2 revealed that  $\alpha$ -carotene interacted with several residues within the cavity of the active site, such as LEU102c, LYS101, ALA58, PHE50, TYR17, VAL14, TRP20 and ALA54 by hydrophobic interactions (Fig. 1A).  $\beta$ -Amyrin interacts with a network of residues, such as TYR 17, TRP 20, PHE 50, ALA 54, LEU 102, and VAL14, by hydrophobic interactions (Fig. 1B). Sulfuretin interacts with key amino acids within the active pocket, such as ALA 54 (distance:2.58) and PHE 51 (distance:6.43)

by hydrogen bonding interactions and VAL 14, TRP 20, PHE 50, and ALA58 by hydrophobic interactions (Fig. 2A). Lem-14, the reference, interacted with TRP 59 (distance: 4.57) by hydrogen bonding interactions; VAL 14, TYR 17, PHE 50, and TRP 20, by hydrophobic interactions (Fig. 2B). According to the Ramachandran plot, VAL14, TYR17, TRP20, PHE51, ASP53, TRP20, PHE50, and ALA58 amino acid residues are in the most favored region (Fig. S1) ([https://kijoms.uokerbala.edu.iq/cgi/editor.cgi?article=3391&window=additional\\_files&context=home](https://kijoms.uokerbala.edu.iq/cgi/editor.cgi?article=3391&window=additional_files&context=home)). Among all the considered phytoconstituents,  $\alpha$ -carotene,  $\beta$ -amyirin, and sulfuretin had relatively high binding capacities with respect to the reference Lem-14 according to sequential computational processes. The common amino acid residues of  $\alpha$ -carotene,  $\beta$ -amyirin, and sulfuretin were LEU102, ALA54, TRP20, VAL14, TYR17, PHE50, ALA58; TYR17, PHE50, TRP20, ALA54, LEU102, VAL14; and ALA58, PHE50, ALA54, TRP20, VAL14, respectively. These molecules fit well into the docking active sites of the target protein.  $\alpha$ -Carotene can be found naturally in *Corbicula sandai* and *Alhagi persarum*. This compound is a type of carotenoid that is known to possess anticancer activity [36]. Sulfuretin, on the other hand, is a natural product found in *Passiflora sexflora*, *Astragalus microcephalus*, and *Rhus verniciflua*. By activating Fas, Caspase-8, and the mitochondrial death pathway, sulfuretin was discovered to trigger apoptosis as a potent cytotoxic agent. Additionally, sulfuretin contributes to preventing cancer cell invasion by blocking NF- $\kappa$ B and downregulating the expression of MMP-9 [37].  $\beta$ -Amyrin is a triterpenoid with multiple pharmacological effects. It is obtained naturally from *Sambucus chinensis* and *Camellia sinensis*. It was shown to exert its cytotoxic action by inducing cell apoptosis and G2/M cycle arrest in a dose-dependent manner. In addition,  $\beta$ -amyirin may stimulate the JNK and p38 signaling pathways [38].

### 3.2. Molecular dynamics simulation data

MD simulations describe various parameters, such as the RMSD, RMSF and residue contact analysis, related to drug-receptor interactions. In the case of  $\alpha$ -carotene, this ligand was less stable during the simulation because the ligand RMSD was near  $8.0 \text{ \AA}$  (Fig. 3A). The protein structure was almost stable because its RMSD was within  $5.0 \text{ \AA}$ . During the simulation, the protein and ligand intermingled at approximately 10 ns, 40 ns, 80 ns and 90 ns. The RMSD of the apoenzyme was nearly  $2.5 \text{ \AA}$ , with very few fluctuations during simulation (Fig. 3B). The protein RMSF plot suggested that

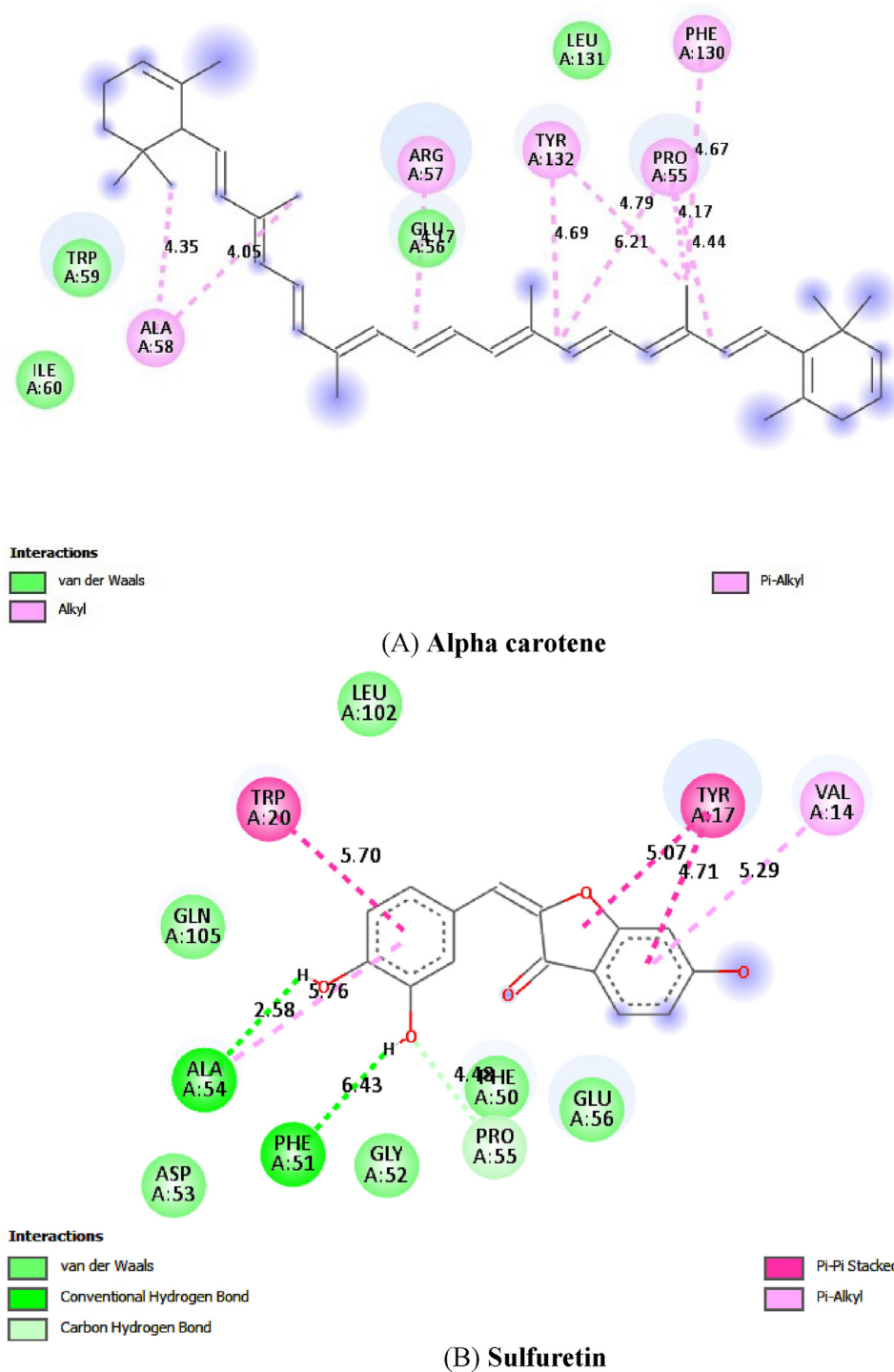


Fig. 1. Molecular docking mechanism of the interactions of alpha carotene and sulfuretin.

some residues exceeded 3.0 Å near 100 residues (Fig. 3C). The green bars near residues 25, 30, 60, and 100 confirmed that at these points, the protein interacted with the ligand molecules. During the simulation, mainly hydrophobic interactions were observed with VAL 14, TYR 17, TRP 20, PRO 28,

LEU 29, PHE 50, ALA 58, TRP 59, ILE 60, PHE 61, and LEU 102 (Fig. 3D–F). In the case of  $\alpha$ -carotene, the RMSD of the apoenzyme reached a static value throughout the analysis without any observable fluctuations, but when  $\alpha$ -carotene interacted with the receptor, it disrupted the structural integrity of

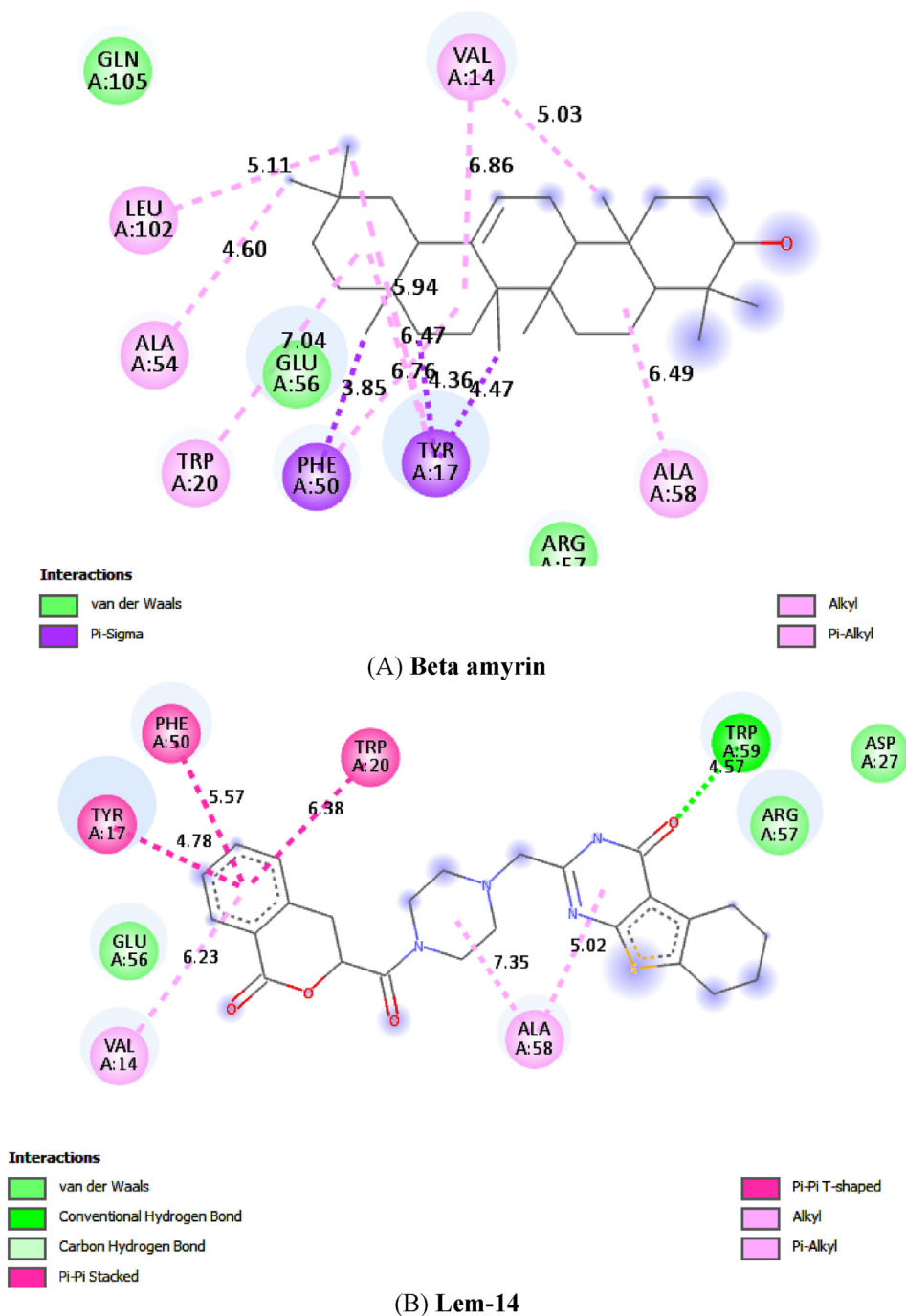


Fig. 2. Molecular docking mechanism of the interactions of Beta amyryn and Lem-14.

the protein. PHE 50 and TRP 20 showed maximum contacts of  $\alpha$ -carotene with the 6UE6 receptor. In the case of  $\alpha$ -carotene, VAL 14, TYR 17, TRP 20, and PHE 50 make strong connections with the receptor within a 4.5 Å distance. Throughout the simulation, a total of 40 atoms of  $\alpha$ -carotene were almost stable [39]. Compared with the RMSD of the apoenzyme shown in Fig. 4A, the RMSD of  $\beta$ -amyryn was stable during the simulation, as the ligand RMSD was

near 4.0 Å with respect to the RMSD plot for the apoenzyme shown in Fig. 3B. Furthermore, the protein structure was stable because its RMSD was within 4.0 Å. During the simulation, the protein and ligand were intermingled throughout the process. In the case of protein RMSF, some residues were within 3.5 Å throughout the simulation time (Fig. 4B). The green bars near residue numbers (10–20), (50–60), and 100 confirmed that at these

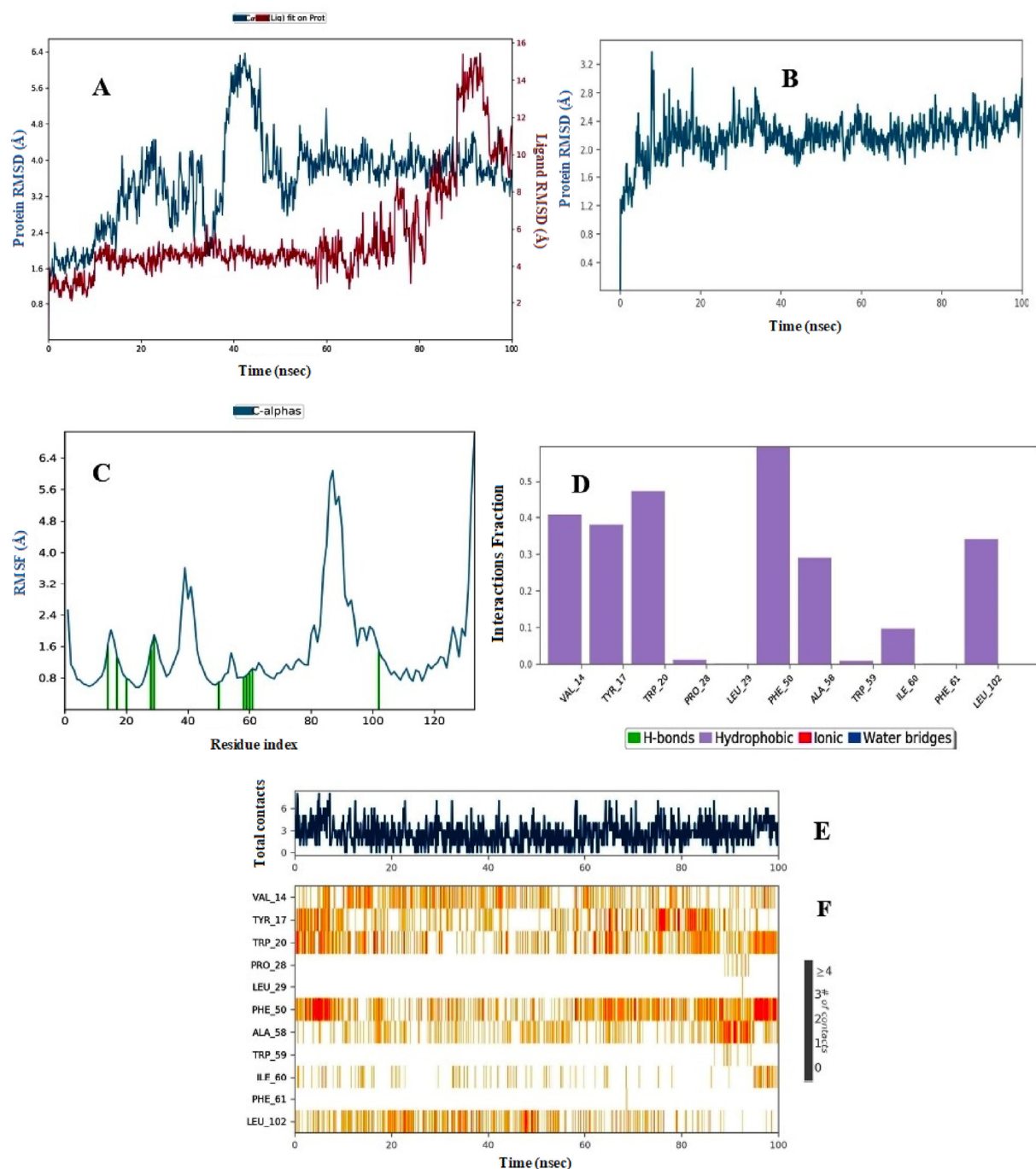


Fig. 3. MD simulation data of  $\alpha$ -carotene interacting with the NSD2 protein (PDB ID: 6UE6). (A) NSD2- $\alpha$ -carotene complex RMSD. (B) RMSD of the NSD2 apoenzyme. (C) RMSF of the  $\alpha$ -carotene complex. (D) Types of interactions in the NSD2- $\alpha$ -carotene complex. Analysis of the (E) timeline and (F) number of NSD2- $\alpha$ -carotene complex contacts.

points, the protein interacted with the ligand molecule. The protein-ligand interactions during the simulation period occurred mostly through hydrophobic interactions, water bridges and hydrogen bonding. VAL 14, TYR 17, TRP 20, PHE 50, ALA 58, TRP 59, ILE 60, and LEU 102 interact with  $\beta$ -amyryn via hydrophobic interactions. LYS

13, SER 15, GLU 56, ARG 57, and TRP 59 interact with  $\beta$ -amyryn via water bridges. TRP 59 interacted with  $\beta$ -amyryn via hydrogen bonding. In the overall interactions, TYR 17, TRP 20 and PHE 50 were the most interactive amino acids during the simulation (Fig. 4C–E). In the case of  $\beta$ -amyryn, TYR 17, TRP 20, and PHE 50 are responsible for the most

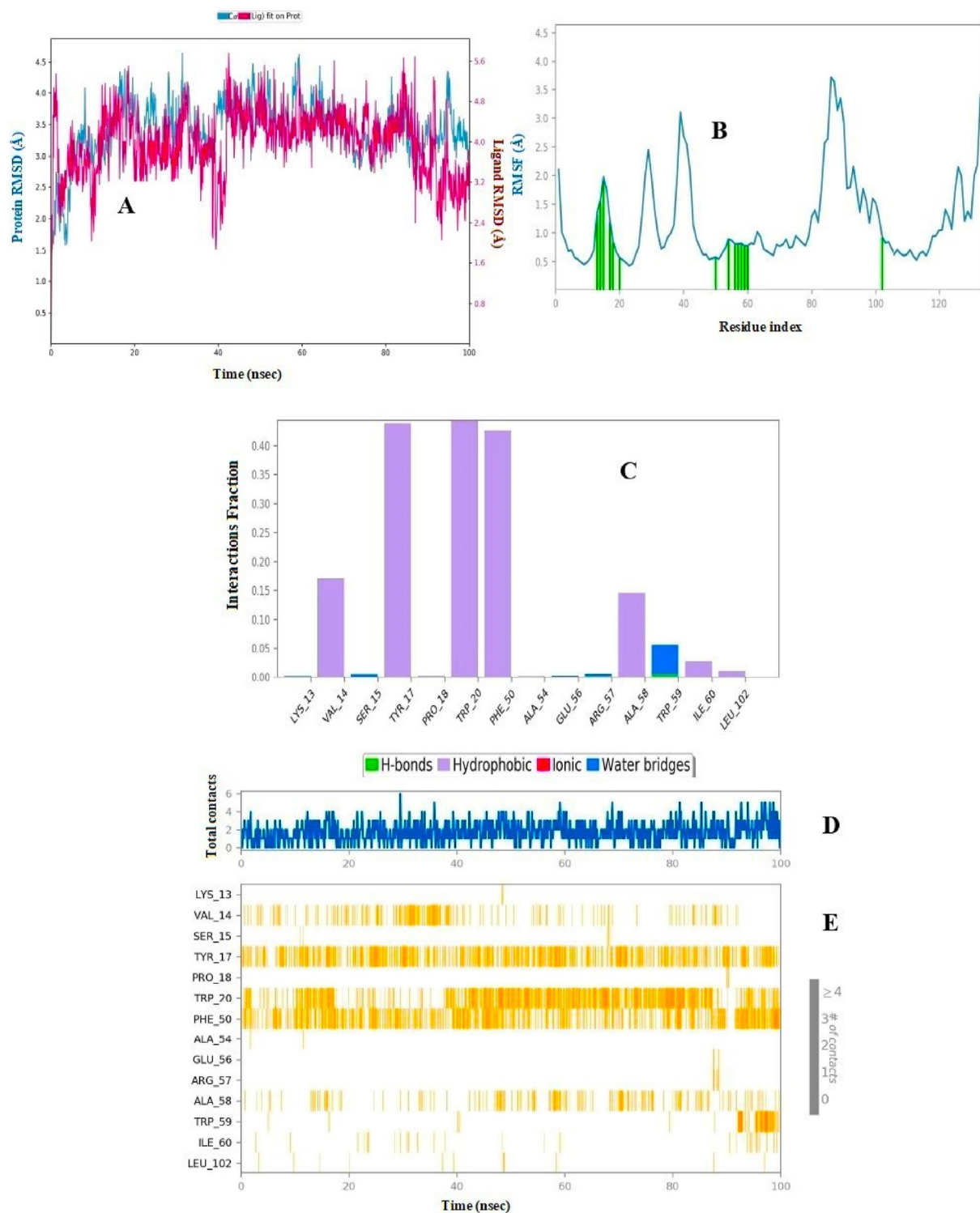


Fig. 4. MD simulation data of the interaction of  $\beta$ -amyrin with the NSD2 protein (PDB ID: 6UE6). (A) NSD2- $\beta$ -amyrin complex RMSD. (B) RMSF of the  $\beta$ -amyrin complex. (C) Types of interactions in the NSD2- $\beta$ -amyrin complex. Analysis of the (D) timeline and (E) number of NSD2- $\beta$ -amyrin complex contacts.

favorable interactions with the receptor within a 4.5 Å distance. Among the 31 atoms of  $\beta$ -amyrin, atoms 4 and 19 presented maximum RMS

fluctuations near 3.0 Å. Sulfuretin was less stable during the simulation, as shown by the ligand RMSD values, which almost reached 8.0 Å (Fig. 5A)

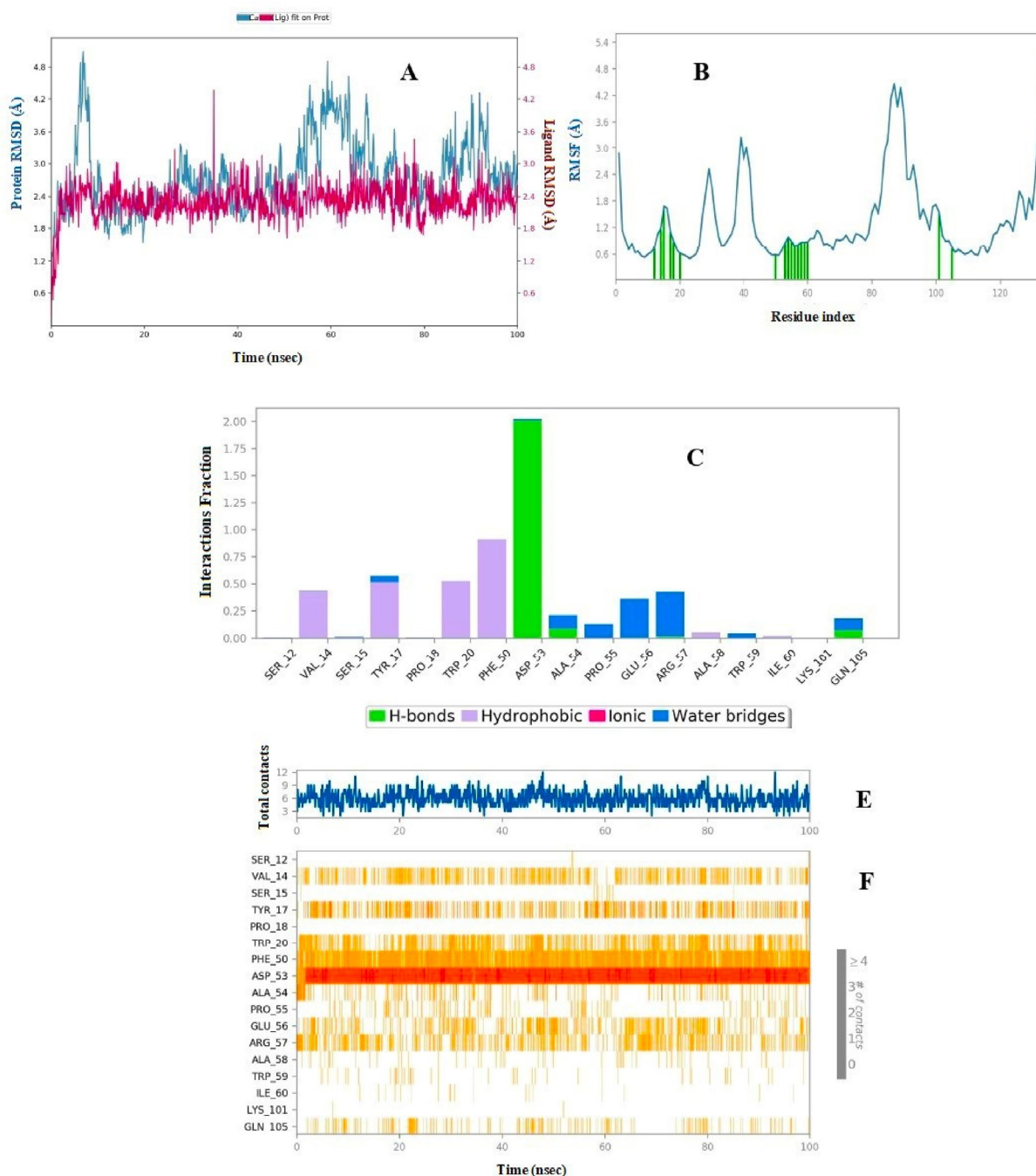


Fig. 5. MD simulation data of the interaction of sulfuretin with the NSD2 protein (PDB ID: 6UE6). (A) NSD2-sulfuretin complex RMSD. (B) RMSF of the sulfuretin complex. (C) Types of interactions in the NSD2-sulfuretin complex. Analysis of the (D) timeline and (E) number of NSD2-Sulphuretin complex contacts.

with respect to the RMSD plot for the apoenzyme shown in Fig. 3B. During the simulation, the protein and ligand intermingled throughout the process except at approximately 60 ns. The protein RMSF indicated that some residues were below 4.0 Å throughout the simulation time (Fig. 5B). The green bars near residue numbers (10–20), (50–60), and

100 confirmed that, at these points, the protein interacted with sulfuretin. The protein-ligand interactions during the simulation were *via* hydrophobic, water bridge and hydrogen bond interactions [40]. SER 12, SER 15, PRO 18, and TRP 20 interact with sulfuretin with hydrophobic interactions. ASP 53, ALA 54, PRO 55, and GLU 56

interact with sulfuretin through water bridges. PHE 50 interacted with sulfuretin by hydrogen bonding. In the overall interactions, sulfuretin interacted with the protein via VAL 14, TRP 20, and PHE 50 using hydrophobic interactions; terminal catechol hydroxyl groups interacted with ASP 53 via negative charge interactions. TYR 17, TRP 20 and PHE 50 were the most interactive amino acids during the simulation (Fig. 5C–E). Remarkably, dynamic analysis of Lem-14 revealed less stable behavior during the simulation, as the ligand RMSD value was near 7.5 Å. In the case of sulfuretin, the RMSD of the apoenzyme reached a static value throughout the analysis without any observable fluctuations, but the interaction of sulfuretin with the receptor disrupted the structural integrity. PHE 50 and ASP53 showed maximum contacts of sulfuretin with the 6UE6 receptor. In the case of sulfuretin, ASP 53 and PHE 50 are responsible for the most favorable interactions with the receptor. In contrast, the RMSD of the ligand–protein complex was more stable, with an average RMSD within 4.2 Å (Fig. 6A) with respect to the RMSD plot for the apoenzyme shown in Fig. 3B. The latter suggested that the protein could shift to a more stable conformation as a result of Lem-14 binding. During the simulation, the protein and ligand intermingled throughout the process except at approximately (0–60) ns and (80–100) ns. The protein RMSF revealed that residues fluctuated below 4.8 Å throughout the simulation time (Fig. 6B). The green bars near residues 10–20, 50–60, 80, and 100 confirmed that at these residues, the protein interacted with the standard Lem-14. The protein–ligand interactions included multiple hydrophobic, water bridge and hydrogen bond interactions during the simulation. Lem-14 interacts with protein residues, including LYS 13, GLY 16, PRO 18, and HIS 47, *via* hydrophobic interactions. Additionally, it formed water–salt bridges with SER 12, VAL 14, TYR 17, LYS 37, PHE 50, ALA 58, ILE 60, PHE 61, and GLN 105. This ligand was also involved in key hydrogen bonding with GLY 16 and ALA 58 (Fig. 6C–E). Similarly, the interactions of Lem-14 with the protein *via* VAL 14, PRO 18, TRP 20, PHE 50, and PHE 61 are the most interactive amino acids during simulation. The RMSD value reflects the point of interaction between the drug and the receptor. The steady RMSD value reflects the perfect coordination between the drug and the receptor [41]. The structural integrity was not significantly hampered by the RMS changes. There is a clear correlation between structural stability and the radius of gyration. ASP 53 interacted with the catechol hydroxyl group via negative charge interactions; ARG 57 interacted

with the terminal hydroxyl group via positive charge interactions; PHE 50 interacted with sulfuretin via  $\pi$ - $\pi$  interactions; and VAL 14 and TRP 20 interacted with the ligand molecule via hydrophobic interactions. Among the 20 atoms of sulfuretin, atom 16 has maximum RMS fluctuations below 1.5 Å [42]. The MD simulation parameters of  $\alpha$ -carotene,  $\beta$ -amyryn, and sulfuretin in complex with NSD2 are within the limit, which highlights the good structural integrity of the ligand molecules upon interaction with the receptor.

### 3.3. FMO analysis data

FMO analysis of  $\alpha$ -carotene,  $\beta$ -amyryn, and sulfuretin revealed corresponding HOMO orbital energy (eV) values of  $-4.59$ ,  $-6.14$ , and  $-5.74$ , respectively. For  $\alpha$ -carotene,  $\beta$ -amyryn, and sulfuretin, the corresponding LUMO orbital energy (eV) values were  $-2.23$ ,  $0.571$ , and  $-2.17$ , respectively. The energy gap between the HOMO and LUMO orbitals reveals the chemical strength and reactivity of a molecule. By taking into account the B3LYP/6-31G(d,p) basis sets, the least energy gap between the HOMO and LUMO orbitals was shown by  $\alpha$ -carotene (2.36 eV), followed by sulfuretin (3.57 eV) and  $\beta$ -amylase (6.71 eV) (Table S5 and Fig. S3) ([https://kijoms.uokerbala.edu.iq/cgi/editor.cgi?article=3391&window=additional\\_files&context=home](https://kijoms.uokerbala.edu.iq/cgi/editor.cgi?article=3391&window=additional_files&context=home)). The HOMO and LUMO orbitals of  $\alpha$ -carotene are situated on the 3,7,12,16-tetramethyl octadeca  $-1,3,5,7,9,11,13,15,17$ - nonaromatic group (linker part of both terminal phenyl groups) [43]. The HOMO and LUMO orbitals of  $\beta$ -amyryn are focused on 3,3,7,8,8a,10a-hexamethyl  $-8$ -propyl-1,2,3,4,4a,6,7,8,8a,9,10,10a-dodecahydrophenanthrene groups. In the case of sulfuretin, the HOMO and LUMO orbitals focus on the (E)-2-(3,4-dihydroxybenzylidene) benzofuran-3(2H)-one group. FMO analysis revealed that the compounds were more stable and reactive in the order of  $\alpha$ -carotene > sulfuretin >  $\beta$ -amyryn. Sulfuretin and  $\alpha$ -carotene had the highest electronegativity and electrophilicity, respectively. Sulfuretin and  $\alpha$ -carotene were shown to be the most reactive compounds. Chemical hardness is closely related to the chemical reactivity and kinetic stability of a molecule [44].

### 3.4. Molecular electrostatic potential (MEP) data

The various colors of the electrostatic potential correspond to different values. The attack zone's potential decreases in the following order: blue, green, yellow, orange, and red. The entire positive area is shown in blue, which is appropriate for

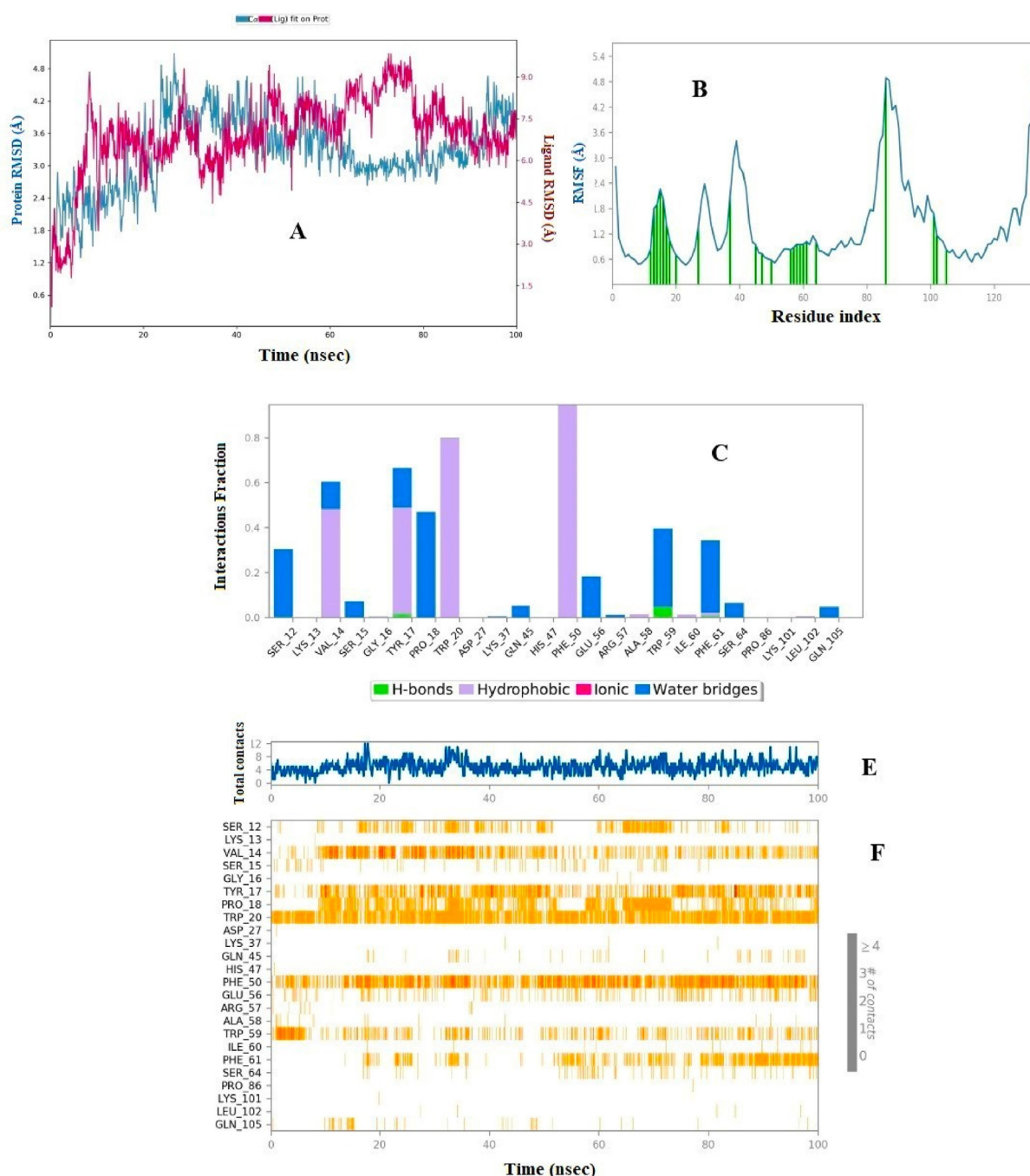


Fig. 6. MD simulation data of Lem-14 interacting with the NSD2 protein (PDB ID: 6UE6). (A) NSD2-Lem-14 complex RMSD. (B) RMSF of the Lem-14 complex. (C) Types of interactions in the NSD2-Lem-14 complex. Analysis of the (D) timeline and (E) number of NSD2-Lem-14 complex contacts.

nucleophilic attack, and the maximal negative area is shown in red, where electrophiles can strike swiftly [45]. Furthermore, there are no possible zones shown in green. The contour MEP map of  $\alpha$ -carotene revealed that the total molecule was green to yellow, which confirmed that there were no potential areas of electrophilic-nucleophilic attack. In the case of  $\beta$ -amyrin, the maximum structure is covered by a neutral green contour zone, but only

the hydroxyl group is shaded with a red-colored zone where an electrophilic attack might occur [46,47]. In the case of sulfuretin, the maximum structure is covered by a neutral green contour zone, and the oxygen atoms present in the structure are shaded in red, where electrophilic attack might occur (Fig. S4) ([https://kijoms.uokerbala.edu.iq/cgi/editor.cgi?article=3391&window=additional\\_files&context=home](https://kijoms.uokerbala.edu.iq/cgi/editor.cgi?article=3391&window=additional_files&context=home)) [48,49].

### 3.5. SAR of $\alpha$ -carotene, $\beta$ -amyirin, and sulfuretin

Alpha-carotene is a carotenoid whose structure is very similar to that of vitamin A. The LogP value of alpha carotene is 13.6 without any hydrogen bond acceptor or donor groups. The nine double bonds present in alpha carotene are responsible for hydrophobic interactions, especially pi–pi interactions. The pentacyclic triterpenoid beta-amyirin is oleanane with a double bond between positions 12 and 13 and a hydroxy group substituting the 3 $\beta$  position. The LogP value of beta-amyirin is 9.2, with 1 hydrogen bond acceptor and 1 donor group. The beta-amyirin structure consists of one hydroxyl group responsible for drug–receptor interactions, and the oleanane structure is associated with hydrophobic interactions. Sulfuretin is a benzofuran-3-one derivative with a LogP value of 2.5, 5 hydrogen bond acceptors and 3 hydrogen bond donor groups. In the structure of sulfuretin, the benzofuranone group is linked with catechol. Three hydroxyl groups and one ketone group are responsible for drug–receptor interactions, and the furan oxygen group also participates in bioactivity.

### 3.6. Calculation of drug likelihood

$\alpha$ -Carotene,  $\beta$ -amyirin, sulfuretin, and lem-14 all passed the drug–likeness parameter, with a minimal oral bioavailability score of 0.55. The permeability and polar surface area of the Caco-2 cells were used to determine the bioavailability score (Abbott bioavailability score) [50]. When the polar surface area of an ion is larger than 150 Å<sup>2</sup>, the bioavailability score is 0.11; when the polar surface area is between 75 and 150 Å<sup>2</sup>, the bioavailability score is 0.56; and when the polar surface area is less than 75 Å<sup>2</sup>, the bioavailability score is 0.85. All the other compounds exhibited good absorption in the gastrointestinal tract, with the exception of  $\beta$ -amyirin and  $\alpha$ -carotene. All other molecules were found to be moderately soluble to extremely soluble, with the exception of  $\alpha$ -carotene and  $\beta$ -amyirin. Lem-14 is a CYP 1A2 inhibitor; CYP 2C19 inhibitors include sulfuretin and Lem-14. Lem-14 is a CYP 2D6 inhibitor (Table S6) ([https://kijoms.uokerbala.edu.iq/cgi/editor.cgi?article=3391&window=additional\\_files&context=home](https://kijoms.uokerbala.edu.iq/cgi/editor.cgi?article=3391&window=additional_files&context=home)). Osiris toxicity prediction data revealed that  $\alpha$ -carotene,  $\beta$ -amyirin, sulfuretin, and Lem-14 are nonmutagenic, nontumorigenic and nonreproductive toxins in nature (Table S7) ([https://kijoms.uokerbala.edu.iq/cgi/editor.cgi?article=3391&window=additional\\_files&context=home](https://kijoms.uokerbala.edu.iq/cgi/editor.cgi?article=3391&window=additional_files&context=home)) [51–57].

## 4. Conclusion

After performing sequential computational studies using berries that target the NSD2 protein, we identified  $\alpha$ -carotene,  $\beta$ -amyirin, and sulfuretin as putative anticancer agents. Alpha carotene has good anticancer activity against lung, liver and skin cancers. *Berberis vulgaris* has shown good anticancer activity against liver, colon, and breast cancer cell lines. *Sambucus nigra* extract has good anti-proliferative effects on ovarian and colorectal cancers. *Morus alba* extract effectively inhibited RAW264.7 macrophages. Beta amyirin has been shown to have good antitumor activity against Hep-G2 liver cancer. Sulfuretin inhibited tumor necrosis factor in a dose-dependent manner. These natural molecules showed maximum docking scores. MD simulation data confirmed that  $\beta$ -amyirin, sulfuretin, and Lem-14 strongly interact with the NSD2 protein without hindering its structural integrity. In conclusion, the bioactive phytochemicals found in berries have great potential for anticancer effects. These phytoconstituents,  $\alpha$ -carotene,  $\beta$ -amyirin, and sulfuritin, are abundantly present in *Berberis vulgaris* (barberry), *Sambucus nigra* (elderberry), and *Morus alba* (white mulberry). These berries have good anticancer properties against lung and prostate cancers, necessitating their high production and cultivation, which can be achieved with agricultural and biotechnological resources. *In vitro* and *in vivo* experiments are necessary to understand the therapeutic potential of these bioactive molecules as NSD2 inhibitors.

### Ethics information

Not applicable. This study is a purely *in silico* analysis with no animal or human subjects.

### Funding

This work was supported by the Uttaranchal University to Supriyo Saha and Research and Publications Cell, University of Chittagong, Bangladesh to SMAK.

### Acknowledgment

This study is supported by the Division of Research & Innovation, Uttaranchal University, Dehradun, India to Supriyo Saha under the seed money grant reference no UU/DRI/SM/2024-25/018 and also the Research and Publication Cell, University of Chittagong, Bangladesh [2023–2024] for support.

## References

- [1] Prinsa, S. Saha, M.Z.H. Bulbul, Y. Ozeki, M.A. Alamri, S.M.A. Kawsar, Flavonoids as potential KRAS inhibitors: DFT, molecular docking, molecular dynamics simulation and ADMET analyses, *J Asian Nat Prod Res* 26 (2024) 955–992, <https://doi.org/10.1080/10286020.2024.2343821>.
- [2] D. Sengupta, L. Zeng, Y. Li, S. Hausmann, D. Ghosh, G. Yuan, T.N. Nguyen, R. Lyu, M. Caporicci, A.M. Benitez, G.L. Coles, V. Kharchenko, I. Czaban, D. Azhibek, W. Fischle, M. Jaremko, I.I. Wistuba, J. Sage, Ł. Jaremko, W. Li, P.K. Mazur, O. Gozani, NSD2 dimethylation at H3K36 promotes lung adenocarcinoma pathogenesis, *Mol Cell* 81 (2021) 4481–4492, <https://doi.org/10.1016/j.molcel.2021.08.034>.
- [3] I. Topchu, R.P. Pangen, I. Bychkov, S.A. Miller, E. Izumchenko, J. Yu, E. Golemis, J. Karanicolas, Y. Bumber, The role of NSD1, NSD2, and NSD3 histone methyltransferases in solid tumors, *Cell Mol Life Sci* 79 (2022) 1–19, <https://link.springer.com/article/10.1007/s00018-022-04321-2>.
- [4] L. Zhang, X. Zha, Recent advances in nuclear receptor-binding SET domain 2 (NSD2) inhibitors: an update and perspectives, *Eur J Med Chem* 250 (2023) 115232, <https://doi.org/10.1016/j.ejmech.2023.115232>.
- [5] R. Chen, Y. Chen, W. Zhao, C. Fang, W. Zhou, X. Yang, M. Ji, The role of methyltransferase NSD2 as a potential oncogene in human solid tumors, *Oncotarget* 13 (2020) 6837–6846, <https://www.tandfonline.com/doi/full/10.2147/OTT.S259873>.
- [6] S. Narang, N.A. Evensen, J. Saliba, J. Pierro, M.L. Loh, P.A. Brown, P. Kolekar, H. Mulder, Y. Shao, J. Easton, X. Ma, A. Tsigirigos, W.L. Carroll, NSD2 E1099K drives relapse in pediatric acute lymphoblastic leukemia by disrupting 3D chromatin organization, *Genome Biol* 24 (2023) 1–25, <https://link.springer.com/article/10.1186/s13059-023-02905-0>.
- [7] B. Baby, P. Antony, R. Vijayan, Antioxidant and anticancer properties of berries, *Crit Rev Food Sci Nutr* 58 (2018) 2491–2507, <https://doi.org/10.1080/10408398.2017.1329198>.
- [8] L. Piao, Y. Gao, X. Xu, Y. Su, Y.D. Wang, J. Zhou, Y. Gao, J. Fang, Q. Li, S. Chang, R. Kong, Discovery of potent small molecule inhibitors of histone lysine methyltransferase NSDs, *Eur J Med Chem* 268 (2024) 116264, <https://doi.org/10.1016/j.ejmech.2024.116264>.
- [9] L. Carlino, P.C. Astles, B. Ackroyd, A. Ahmed, C. Chan, G.W. Collie, I.L. Dale, D.H. O'Donovan, C. Fawcett, P. di Fruscia, A. Gohlke, X. Guo, J. Hao-Ru Hsu, B. Kaplan, A.G. Milbradt, S. Northall, D. Petrović, E.L. Rivers, E. Underwood, A. Webb, Identification of novel potent NSD2-PWWP1 ligands using structure-based design and computational approaches, *J Med Chem* 67 (2024) 8962–8987, <https://doi.org/10.1021/acs.jmedchem.4c00215>.
- [10] S. Skrovankova, D. Sumczynski, J. Mlcek, T. Jurikova, J. Sochor, Bioactive compounds and antioxidant activity in different types of berries, *Int J Mol Sci* 16 (2015) 24673–24706, <https://doi.org/10.3390/ijms161024673>.
- [11] G. Schmeda-Hirschmann, F. Jiménez-Aspee, C. Theoduloz, A. Ladio, Patagonian berries as native food and medicine, *J Ethnopharmacol* 241 (2019) 111979, <https://doi.org/10.1016/j.jep.2019.111979>.
- [12] N. Li, H. Yang, K. Liu, L. Zhou, Y. Huang, D. Cao, Y. Li, Y. Sun, A. Yu, Z. Du, F. Yu, Y. Zhang, B. Wang, M. Geng, J. Li, B. Xiong, S. Xu, X. Huang, T. Liu, Structure-based discovery of a series of NSD2-PWWP1 inhibitors, *J Med Chem* 65 (2022) 9459–9477, <https://doi.org/10.1021/acs.jmedchem.2c00709>.
- [13] D. Dilworth, R.P. Hanley, R. Ferreira de Freitas, A. Allali-Hassani, M. Zhou, N. Mehta, M.R. Marunde, S. Ackloo, R. Arminda C. Machado, A.K. Yazdi, D.D.G. Owens, V. Vu, D.Y. Nie, M. Alqazzaz, E. Marcon, F. Li, I. Chau, A. Bolotokova, S. Qin, M. Lei, Y. Liu, M.M. Szcwycyk, A. Dong, S. Kazemzadeh, T. Abramyan, I.K. Popova, N.W. Hall, M.J. Meiners, M.A. Cheek, E. Gibson, D. Kireev, J.F. Greenblatt, M.C. Keogh, J. Min, P.J. Brown, M. Vedadi, C.H. Arrowsmith, D. Barsyte-Lovejoy, L.I. James, M. Schapira, A chemical probe targeting the PWWP domain alters NSD2 nucleolar localization, *Nat Chem Biol* 18 (2022) 56–63, <https://www.nature.com/articles/s41589-021-00898-0>.
- [14] Y. Shen, M. Morishit, D. Lee, S. Kim, T. Lee, D.E.H.F. Mevius, Y. Roh, E. di Luccio, Identification of LEM-14 inhibitor of the oncoprotein NSD2, *Biochem Biophys Res Commun* 508 (2019) 102–108, <https://doi.org/10.1016/j.bbrc.2018.11.037>.
- [15] A.S. Alamri, A.S. Alawam, M.M. Alshahrani, S.M.A. Kawsar, Prinsa, S. Saha, Establishing the role of iridoids as potential kirsten rat sarcoma viral oncogene homolog G12C inhibitors using molecular docking; molecular docking simulation; molecular mechanics Poisson-Boltzmann surface area; frontier molecular orbital theory; molecular electrostatic potential; and absorption, distribution, metabolism, excretion, and toxicity analysis, *Molecules* 28 (2023) 5050, <https://doi.org/10.3390/molecules28135050>.
- [16] S. Akter, B.Y. Alhatlani, E.M. Abdallah, S. Saha, J. Ferdous, M.E. Hossain, F. Ali, S.M.A. Kawsar, Exploring cinnamoyl-substituted mannopyranosides: synthesis, evaluation of antimicrobial properties, and molecular docking studies targeting H5N1 influenza A virus, *Molecules* 28 (2023) 8001, <https://doi.org/10.3390/molecules28248001>.
- [17] P. Kumar, P. Kumar, A. Shrivastava, M.A. Dar, K.B. Lokhande, N. Singh, A. Singh, R. Velayutham, D. Mandal, Immunoinformatics-based multi-epitope containing fused polypeptide vaccine design against visceral leishmaniasis with high immunogenicity and TLR binding, *Int J Biol Macromol* 253 (2023) 127567, <https://doi.org/10.1016/j.ijbiomac.2023.127567>.
- [18] K. Lokhande, N.K. Nawani, S.K. Venkateswara, S. Pawar, Biflavonoids from *Rhus succedanea* as probable natural inhibitors against SARS-CoV-2: a molecular docking and molecular dynamics approach, *J Biomol Struct Dyn* 40 (2022) 4376–4388, <https://doi.org/10.1080/07391102.2020.1858165>.
- [19] T. Shamsuddin, M.A. Hosen, M.S. Alam, T.B. Emran, S.M.A. Kawsar, Uridine derivatives: antifungal, PASS outcomes, ADME/T, drug-likeness, molecular docking and binding energy calculations, *Med. Sci. Int. Med. J.* 10 (2021) 1373–1386, <https://doi.org/10.5455/medscience.2021.05.175>.
- [20] S.M.A. Kawsar, M.A. Hosen, T.S. Chowdhury, K.M. Rana, Y. Fujii, Y. Ozeki, Thermochemical, PASS, molecular docking, drug-likeness and in silico ADMET prediction of cytidine derivatives against HIV-1 reverse transcriptase, *Rev. de. Chim.* 72 (2021) 159–178, <https://doi.org/10.37358/Rev.Chim.1949>.
- [21] K.B. Lokhande, S. Doiphode, R. Vyas, K.V. Swamy, Molecular docking and simulation studies on SARS-CoV-2 M<sup>Pro</sup> reveals Mitoxantrone, Leucovorin, Birinapant, and Dynasore as potent drugs against COVID-19, *J Biomol Struct Dyn* 39 (2021) 7294–7305, <https://doi.org/10.1080/07391102.2020.1805019>.
- [22] A. Abdou, F.E. Maaghloud, A. Elmakssoudi, A. Aboulmouhajir, J.J. Eddine, M. Dakir, Synthesis of eugenol derivative by the ring opening of epoxide eugenol and its analysis through chemical reactivity: a DFT approach, *Nat Prod Res* 38 (2024) 1099–1107, <https://doi.org/10.1080/14786419.2022.2132242>.
- [23] S. Rochlani, M. Bhatia, S. Rathod, P. Choudhari, R. Dhavale, Exploration of limonoids for their broad-spectrum antiviral potential *via* DFT, molecular docking and molecular dynamics simulation approach, *Nat Prod Res* 38 (2024) 891–896, <https://doi.org/10.1080/14786419.2023.2202398>.
- [24] S. Saha, V.J. Prinsa, A.K. Mahato, S. Srivastava, K. Dobhal, S.M. A Kawsar, In silico assessment of the role of iridoid in the treatment of zika and influenza virus infection, *Phil. J. Sci.* 152 (2023) 1953–1988, <https://doi.org/10.56899/152.05.35>.
- [25] M.A. Hosen, A. Alam, M. Islam, Y. Fujii, Y. Ozeki, S.M.A. Kawsar, Geometrical optimization, PASS prediction, molecular docking, and in silico ADMET studies of thymidine derivatives against FimH adhesin of *Escherichia coli*, *Bulg Chem Commun* 53 (2021) 327–342, <https://doi.org/10.34049/bcc.53.3.5375>.

- [26] S.M.A. Kawsar, M.A. Hosen, Y. El Bakri, S. Ahmad, S.T. Affi, S. Goumri-Said, In silico approach for potential antimicrobial agents through antiviral, molecular docking, molecular dynamics, pharmacokinetic and bioactivity predictions of galactopyranoside derivatives, Arab. J. Basic. Appl. Sci. 29 (2022) 99–112, <https://doi.org/10.1080/25765299.2022.2068275>.
- [27] N. Chaachouay, L. Zidane, Plant-Derived Natural Products: a source for drug discovery and development, Drug, Drug. Cand. 3 (2024) 184–207, <https://doi.org/10.3390/ddc3010011>.
- [28] N. Akter, S. Saha, M.A. Hossain, K.M. Uddin, A.R. Bhat, S. Ahmed, S.M.A. Kawsar, Acylated glucopyranosides: FTIR, NMR, FMO, MEP, molecular docking, dynamics simulation, ADMET and antimicrobial activity against bacterial and fungal pathogens, Chem. Phys. Impact 9 (2024) 100700, <https://doi.org/10.1016/j.chphi.2024.100700>.
- [29] Z. Zhao, J. Chen, F.F. Ci, H. Pang, N. Cheng, A. Xing,  $\alpha$ -Carotene: a valuable carotenoid in biological and medical research, J Sci Food Agric 102 (2022) 5606–5617, <https://doi.org/10.1002/jsfa.11966>.
- [30] A.H.E. Hassan, C.Y. Wang, C.J. Lee, H.R. Jeon, Y. Choi, S. Moon, C.H. Lee, Y.J. Kim, S.B. Cho, K. Mahmoud, S.M. El-Sayed, S.K. Le, Y.S. Lee, Repurposing Synthetic congeners of a natural product aureone unveils a lead antitumor agent inhibiting folded p-loop conformation of MET receptor tyrosine kinase, Pharmaceuticals 16 (2023) 1597, <https://doi.org/10.3390/ph16111597>.
- [31] S. Wen, D. Gu, H. Zeng, Antitumor effects of beta-amyrin in Hep-G2 liver carcinoma cells are mediated via apoptosis induction, cell cycle disruption and activation of JNK and P38 signalling pathways, J. BUON. 23 (2018) 965–970. PMID: 30358200.
- [32] A.K. Singh, S. Kumar, Naringin dihydrochalcone potentially binds to catalytic domain of matrix metalloproteinase-2: molecular docking, MM-GBSA, and molecular dynamics simulation approach, Nat Prod Res 37 (2023) 1851–1855, <https://doi.org/10.1080/14786419.2022.2118746>.
- [33] R.F. de Freitas, Y. Liu, M.M. Szweczyk, N. Mehta, F. Li, D. McLeod, C. Zepeda-Velázquez, D. Dilworth, R.P. Hanley, E. Gibson, P.J. Brown, R. Al-Awar, L.I. James, C.H. Arrowsmith, D. Baryshte-Lovejoy, J. Min, M. Vedadi, M. Schapira, A. Allali-Hassani, Discovery of small-molecule antagonists of the PWWP domain of NSD2, J Med Chem 64 (2021) 1584–1592, <https://doi.org/10.1021/acs.jmedchem.0c01768>.
- [34] S.W. Park, B.H. Lee, S.H. Song, M.K. Kim, Revisiting the Ramachandran plot based on statistical analysis of static and dynamic characteristics of protein structures, J Struct Biol 215 (2023) 107939, <https://doi.org/10.1016/j.jsb.2023.107939>.
- [35] S.S. Sheik, P. Sundararajan, A.S.Z. Hussain, K. Sekar, Ramachandran plot on the web, Bioinformatics 18 (2002) 1548–1549, <https://doi.org/10.1093/bioinformatics/18.11.1548>.
- [36] M.D. Hanwell, D.E. Curtis, D.C. Lonie, T. Vandermeersch, E. Zurek, G.R. Hutchison, Avogadro: an advanced semantic chemical editor, visualization, and analysis platform, J Cheminf 4 (2012) 1–17. <https://link.springer.com/article/10.1186/1758-2946-4-17>.
- [37] N.M. O'Boyle, M. Banck, C.A. James, C. Morley, T. Vandermeersch, G.R. Hutchison, Open Babel: an open chemical toolbox, J Cheminf 3 (2011) 1–14. <https://link.springer.com/article/10.1186/1758-2946-3-33>.
- [38] S.M.A. Kawsar, N.S. Munia, S. Saha, Y. Ozeki, In silico pharmacokinetics, molecular docking and molecular dynamics simulation studies of nucleoside analogs for drug discovery- A mini-review, Mini Rev Med Chem 24 (2024) 1070–1088, <https://doi.org/10.2174/0113895575258033231024073521>.
- [39] D.S. Goodsell, M.F. Sanner, A.J. Olson, S. Forli, The AutoDock suite at 30, protein, Sci 30 (2021) 31–43, <https://doi.org/10.1002/pro.3934>.
- [40] O. Trott, A.J. Olson, AutoDockVina: improving the speed and accuracy of docking with a new scoring function, efficient optimization, and multithreading, J Comput Chem 31 (2010) 455–461, <https://doi.org/10.1002/jcc.21334>.
- [41] S.A. Hollingsworth, R.O. Dror, Molecular dynamics simulation for all, Neuron 99 (2018) 1129–1143, <https://doi.org/10.1016/j.neuron.2018.08.011>.
- [42] N. Akter, L. Bourougaa, M. Ouassaf, R.C. Bhowmic, K.M. Uddin, A.R. Bhat, S. Ahmed, S.M.A. Kawsar, Molecular docking, ADME-Tox, DFT and molecular dynamics simulation of butyryl glucopyranoside derivatives against DNA gyrase inhibitors as antimicrobial agents, J Mol Struct 1307 (2024) 137930, <https://doi.org/10.1016/j.molstruc.2024.137930>.
- [43] E. Harder, W. Damm, J. Maple, C. Wu, M. Reboul, J.Y. Xiang, L. Wang, D. Lupyan, M.K. Dahlgren, J.L. Knight, J.W. Kaus, D.S. Cerutti, G. Krilov, W.L. Jorgensen, R. Abel, R.A. Friesner, OPLS3: a Force Field providing broad coverage of drug-like small molecules and proteins, J Chem Theor Comput 12 (2016) 281–296, <https://doi.org/10.1021/acs.jctc.5b00864>.
- [44] A.U. Islam, H. Hadni, F. Ali, A. Abuzreda, S.M.A. Kawsar, Synthesis, antimicrobial activity, molecular docking, molecular dynamics simulation, and ADMET properties of the mannopyranoside derivatives as antimicrobial agents, J Taibah Univ Sci 18 (2024) 2327101, <https://doi.org/10.1080/16583655.2024.2327101>.
- [45] J. Yu, N.Q. Su, W. Yang, Describing chemical reactivity with frontier molecular orbitals, JACS. Au. 2 (2022) 1383–1394, <https://doi.org/10.1021/jacsau.2c00085>.
- [46] A.U. Islam, T. Serseg, K. Benarous, F. Ahmed, S.M.A. Kawsar, Synthesis, antimicrobial activity, molecular docking and pharmacophore analysis of new propionyl mannopyranosides, J Mol Struct 1292 (2023) 135999, <https://doi.org/10.1016/j.molstruc.2023.135999>.
- [47] A.C.C. Jr, G.F. Ondar, O. Versiane, J.M. Ramos, T.G. Santos, A.A. Martin, L. Raniero G.G.A. Bussi, C.A.T. Soto, DFT: B3LYP/6-311G. p) Vibrational analysis of bis-(diethylthiocarbamate)zinc(II) and natural bond orbitals, Spectrochim. Acta. A. Mol. Biomol. Spectrosc. 105 (2013) 251–258, <https://doi.org/10.1016/j.saa.2012.11.097>.
- [48] M.J. Perri, S.H. Weber, Web-based job submission interface for the GAMESS computational chemistry program, J Chem Educ 91 (2014) 2206–2208, <https://doi.org/10.1021/ed5004228>.
- [49] L. Liu, L. Miao, L. Li, F. Li, Y. Lu, Z. Shang, J. Chen, Molecular electrostatic potential: a new tool to predict the lithiation process of organic battery materials, J Phys Chem Lett 9 (2018) 3573–3579, <https://doi.org/10.1021/acs.jpcclett.8b01123>.
- [50] A. Daina, O. Michielin, V. Zoete, SwissADME: a free web tool to evaluate pharmacokinetics, drug-likeness and medicinal chemistry friendliness of small molecules, Sci Rep 7 (2017) 42717. <https://www.nature.com/articles/srep42717>.
- [51] P. Ertl, A. Schuffenhauer, Estimation of synthetic accessibility score of drug-like molecules based on molecular complexity and fragment contributions, J Cheminf 1 (2009) 8. <https://link.springer.com/article/10.1186/1758-2946-1-8/metrics>.
- [52] S. Sultana, M.A. Hossain, S. Biswas, M.A. Saleh, F. Ali, S.M.A. Kawsar, Chemical reactivity, molecular electrostatic potential, FTIR, NMR, *in vitro*, and *in silico* studies of mannopyranoside derivatives: 3-Nitrobenzoylation leads to improved antimicrobial activity, Chem. Phys. Impact 9 (2024) 100692, <https://doi.org/10.1016/j.chphi.2024.100692>.
- [53] T. Murakoshi, H. Nishino, Y. Satomi, J. Takayasu, T. Hasegawa, H. Tokuda, A. Iwashima, J. Okuzumi, H. Okabe, H. Kitano, I. Ryoza, Potent preventive action of alpha-carotene against carcinogenesis: spontaneous liver carcinogenesis and promoting stage of lung and skin carcinogenesis in mice are suppressed more effectively by alpha-carotene than by beta-carotene, Cancer Res 52 (1992) 6583–6587. PMID: 1423303.
- [54] A.E. Abd El-Wahab, D.A. Ghareeb, E.E. Sarhan, M.M. Abu-Serie, M.A. El Demellawy, *In vitro* biological assessment of Berberis vulgaris and its active constituent, berberine: anti-oxidants, anti-acetylcholinesterase, anti-diabetic and

- anticancer effects, *BMC Compl Alternative Med* 13 (2013) 218, <https://doi.org/10.1186/1472-6882-13-218>.
- [55] A.E. Stępień, J. Trojniak, J. Tabarkiewicz, Health-Promoting properties: anti-inflammatory and anticancer properties of *Sambucus nigra* L. Flowers and fruits, *Molecules* 28 (2023) 6235, <https://doi.org/10.3390/molecules28176235>.
- [56] H.J. Eo, J.H. Park, G.H. Park, M.H. Lee, J.R. Lee, J.S. Koo, J.B. Jeong, Anti-inflammatory and anti-cancer activity of mulberry (*Morus alba* L.) root bark, *BMC Compl Alternative Med* 14 (2014) 1–9, <https://doi.org/10.1186/1472-6882-14-200>.
- [57] J.S. Shin, Y.M. Park, J.H. Choi, H.J. Park, M.C. Shin, Y.S. Lee, K.T. Lee, Sulfuretin isolated from heartwood of *Rhus verniciflua* inhibits LPS-induced inducible nitric oxide synthase, cyclooxygenase-2, and pro-inflammatory cytokines expression via the down-regulation of NF-kappaB in RAW 264.7 murine macrophage cells, *Int Immunopharm* 10 (2010) 943–950, <https://doi.org/10.1016/j.intimp.2010.05.007>.